3rd URSI AT-AP-RASC, Gran Canaria, 29 May – 3 June 2022

Self-Dual Power Splitters for Wide-Scan, Wideband Phased Array Applications

Roee Geva and Raphael Kastner*
School of Electrical Engineering, Tel Aviv University, Tel Aviv 69978, Israel

Abstract

Self-dual media (SDM) have been shown to enable the design of inherently reflection-less radiating elements for phased array applications with extreme scanning demands. As a natural continuation to this work, we lay here the foundations for a complete SDM-based feeding and beamforming network system in the form of SDM-based power splitters. The scope of this work includes simulations and optimization of the splitters in several forms, as well as a transition from a conventional microstrip to SDM.

1 Introduction

Recently, we have applied the remarkable property of non-reflection from self-dual media (SDM) [1] to the design of inherently matched phased arrays over large scan range and bandwidth [2]. We have shown the mechanism by which self-duality is helpful in producing slowly-varying element pattern that translates to very low active reflection coefficient over wide scan and frequency ranges [3]. As a natural continuation to this work, we proceed to the design of SDM-based power splitters in several configurations, including transitions from conventional microstrip lines, with an eye for future design of beam forming networks as part of comprehensive phased array systems. In general, SDM are slab-like materials with the following property (1), and will exhibit inherently zero backscatter when subject to a normally incident plane wave:

$$\varepsilon_r(x,y) = \mu_r(-y,x), \tag{1}$$

at any cross-sectional plane $z = \text{const.}$ within the slab. Condition(1) merely defines a class of planar unit cells that remain unchanged if 1) the structure is rotated 90^0 about the z-axis, and 2) any electric material with relative permittivity ε_r is replaced by a magnetic material with the relative permeability $\mu_r = \varepsilon_r$, and vice versa. An SDM-based radiating element [3] is shown in Fig. 1. In this element, most of the energy is funneled through the central bore with no reflections. The bore can be deeply sub-wavelength. The materials of choice are near-PECs and near-PMCs, assuming that their properties obey (1) across the entire operating frequency range. The outer dimensions can also be very small compared with the wavelength. This element is to be fed by a conventional microstrip line and incorporated into a power dividing configuration.

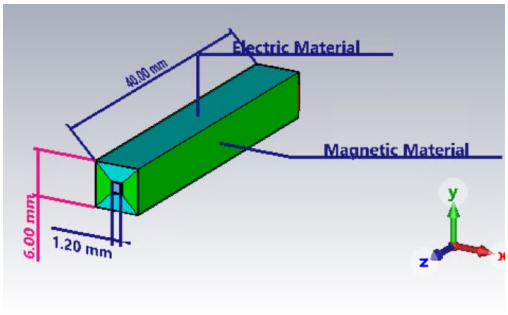

Figure 1. . SDM radiating element. The top and bottom (blue) prism-like regions are near-PEC with $\varepsilon'_r = 1$ and $\sigma_e = 10^7$ S/m and the complementary side (green) regions are near-PMC with $\mu'_r = 1$ and $\sigma_h = 1.42 \cdot 10^{12}\ \Omega/\text{m}$, such that $\varepsilon''_r = \mu''_r \gg 1$. As seen in the Figure, the size of the bore is one-fifth of the side of the element,

2 SDM Power Splitters

Radiating elements of the type in Fig. 1, when incorporated into a phased array system, would be fed by a power dividing network. Rather than building a conventional splitter and add transitions into individual elements, we propose new types of splitters in the SDM environment. Out of several possible structures, we present two options as follows.

2.1 Option I: Direct-Aperture-Feed Splitter

The Direct-Aperture-Feed (DAF) splitter is capable of splitting the energy in uniformly in a $1:16$ ratio. It comprises three main levels, all SDM, as seen in Fig. 2(a):

1. The "entrance level" is a section of the SDM element of the type in Fig. 1, serves as the feed that includes the input port plane;
2. The "tapering level", that matches gradually the entrance level to the splitting aperture via a TEM mode;
3. The splitting aperture, made of a $2^N \times 2^M$ array of SDM elements that may have different external dimensions than the feeder, seen also in Fig. 2(b). In the following examples, all the central bores share equal dimensions to maintain uniform amplitude distribution on the splitting aperture. We have also chosen $N = M = 2$ as in this figure.

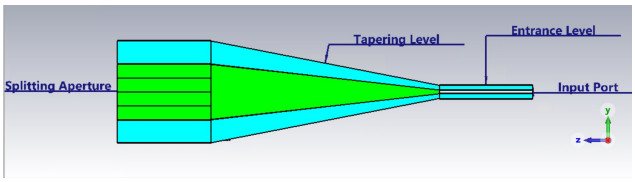

(a) Side view

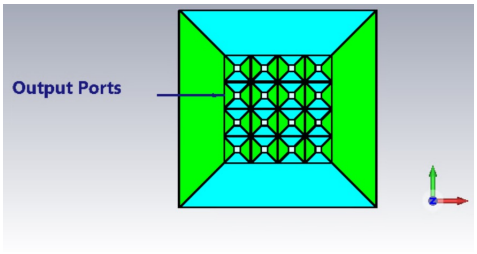

(b) Front view

Figure 2. (a) DAF levels; (b) DAF splitting aperture. Electrical and magnetic parameters of each of the 16 elements are the same as in Fig. 1, however external dimensions may be different.

The DAF splitter achieves a $1:2^{N+M}$ power division (1 : 16 in Fig. 2(b)) in one stage, making it relatively compact and easy to design and model. Moreover, theoretically, there is no limitation on the operational bandwidth, thus a single splitting network may become useful for several applications.

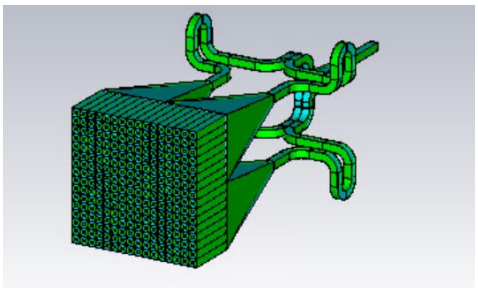

Figure 3. Representative example of splitter model involving bends and tapers to reduce the overall tapering length.

Total dimensions of the tapering level can be further reduced using E/H-plane bends. Also, although not strictly SDM, 45^0 corners have shown good results. Example of such a splitter model mixing bends and tapering level horn are shown in Fig. 3. The effect of linear tapering length on power-division performance has been investigated in two aspects, viz. S-parameter performance and radiation efficiency of the aperture when all aperture elements are open ended and radiate. As a rule-of-thumb, for linear tapering, reasonable performance will be achieved when the taper length is twice the aperture size. S-parameter performance of both $1:16$ ($N=M=2$) and $1:64$ ($N=M=3$) splitters with taper length as per the above mentioned rule-of-thumb are shown in Fig. 4. As expected, inherently good matching is achieved all over the operational bandwidth. For example, for the 1 : 64 splitter with the 100 mm taper length (Figs 4(c) and 4(d)), the peak-to-peak deviations is 1.6 dB and 48^0. In other words, the average difference between adjacent elements is about 0.2 dB and 6^0. / Performance for

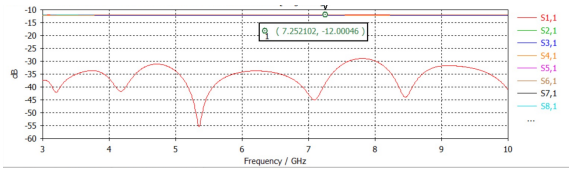

(a) S-parameter anplitudes, 1 : 16 splitter.

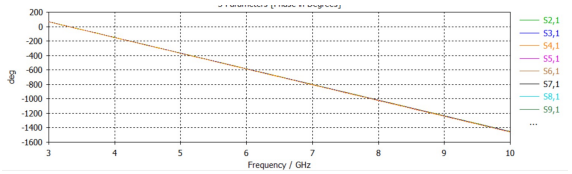

(b) S-parameter phase, 1 : 16 splitter.

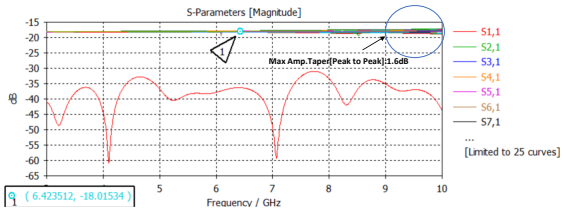

(c) S-parameter anplitudes, 1 : 64 splitter.

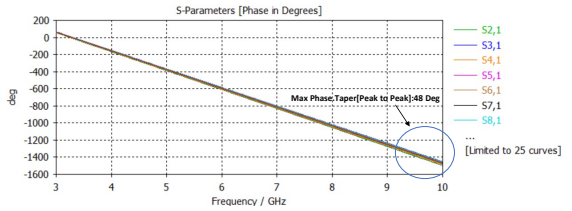

(d) S-parameter phase, 1 : 64 splitter.

Figure 4. S-parameter performance for 1 : 16 and 1 : 64 DAF splitters. In (a) and (b), all ports are shown. In (c) and (d), ports have been grouped, each group sharing the same distance from the center of the aperture and the same amplitude and phase. Worst case for the 1 : 64 splitter occurs at the highest frequency, marked with circles in (c) and (d).

two tapering lengths, 15 mm and 50 mm, are shown for the 1 : 16 splitter in Fig 5. As one may expect, results improve with longer tapers.

2.2 Option II: Perturbed Splitter

Th perturbed splitter, proposed here, provides flexible geometrical arrangement, as opposed to the DAF where all outputs are on the same plane. This splitter is composed of a main SDM element of the type shown in Fig. 1, onto which external SDM perturbations are drilled as in Fig. 6. The perturbations are again SDM element of the same type, except much narrower, and are referred herein as Secondary SDM. Energy is coupled from the main bore to the secondary SDM. The output ports are located at the tip of secondary-SDM. The basic structure is shown in Figs. 6(a)

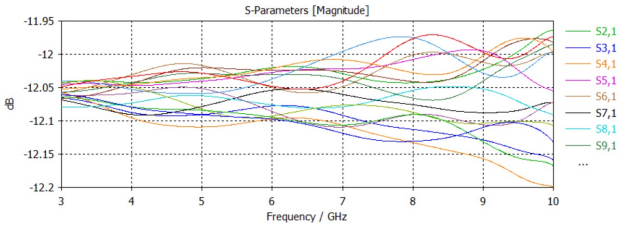

(a) S parameters amplitude (dB) for a 50 mm taper.

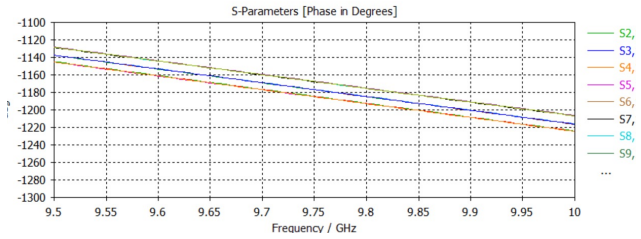

(b) S-parameters phase (deg) for a 50 mm taper.

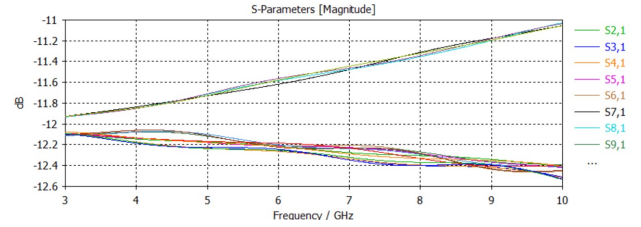

(c) S-parameters amplitude (dB) for a 15 mm taper.

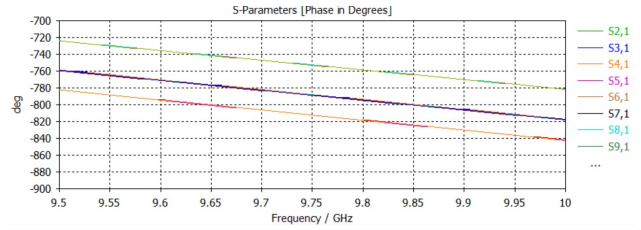

(d) S-parameters phase (deg) for a 15 mm taper.

Figure 5. Blowups of S-parameter performance for two lengths of taper in the 1 : 16 splitter.

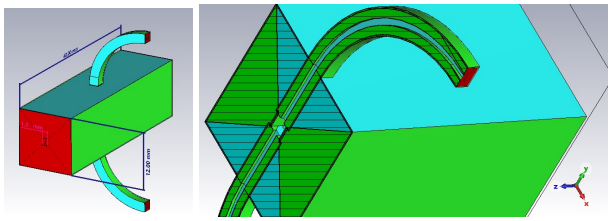

(a) 3D configuration. (b) 3D model of the junction.

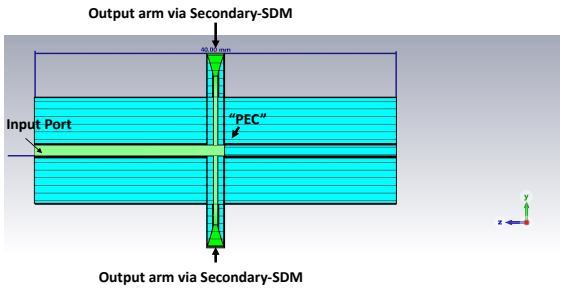

(c) Side cross section.

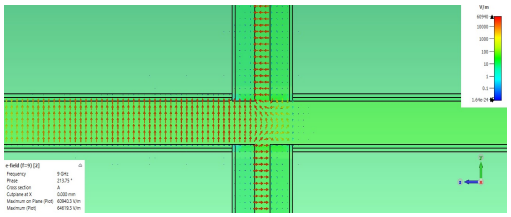

(d) Blown up profile of the E-field in the main-to-secondary SDM junction

Figure 6. perturbed splitter configuration.

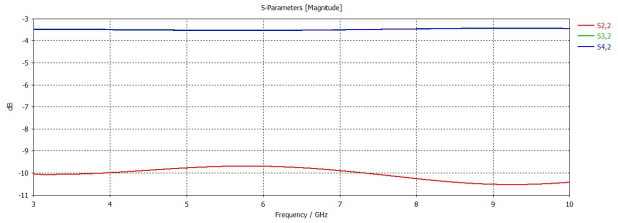

Figure 7. S-parameters for the perturbed Splitter.

and 6(b). The electric and magnetic fields are perturbted at the intersection with the secondary-SDM, causing them to couple into the drills, see Figs. 6(c) and 6(d) that show how the entire power is essentially coupled into the secondary SDM, with the two outputs being out of phase. This device also operates over a wide frequency band, as can be seen in Fig. 7, showing a VSWR of approximately 2:1 over the entire $3-10$ GHz range. Simulation for the exact same structure for the $3-20$ GHz have shown similar results.

3 Microstrip to SDM Transition

To connect with conventional RF devices, a transition is proposed as follows. We note that the bore within the radiating element of Fig. 1 supports a TEM mode with a characteristic impedance of $Z_c = 377\ \Omega$. Since microstrip lines with the same impedance are impractical we are proposing a TEM horn [4] as a tapered transition between the two lines, see Fig. 8. The aperture of the TEM-horn that interfaces directly with the SDM should support the fundamental TEM mode only. The cutoff wavelength of the next higher order mode is given by $\lambda_c = 2d$, when d is the TEM-horn height. In our operational bandwidth of $3-10$ GHz, the dimensions of this output port are limited to 15 mm. As the impedance at any point along the horn is given by

$$Z_{\text{horn}} = 120\pi \frac{d(z)}{W(z)},$$

the requirement for 377 Ω line impedance at its output port forces $d_{\text{out}} = W_{\text{out}}$. The width and height at any other point along the TEM-horn are governed by an exponential taper. The TEM-horn may be fed in the standard way by using, e.g., baluned-microstrip line. With the height and width at the output already set, the sole unknown left to determine

is the input impedance which should fit the feeding waveguide. In this proposed feeding method, the entrance level for each SDM element is constructed of a standard waveguide (such as baluned-microstrip). Other feeding methods such as gap waveguides are under consideration.

The SDM itself, now uniformly illuminated by a normal incident plane-wave, is transparent to this feeding structure. Representative *S*-parameter results for the TEM-horn alone is shown in Fig. 9(a) for an input impedance of 130 Ω, while the SDM-to-TEM-horn level performance are shown in Fig. 9(b). An example of feeding the TEM-horn-SDM combination via a microstip line is shown in Fig. 9(c). In this case, the performance is determined mostly by the microstrip-TEM-horn interface.

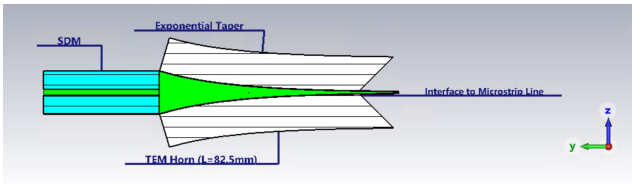

(a)

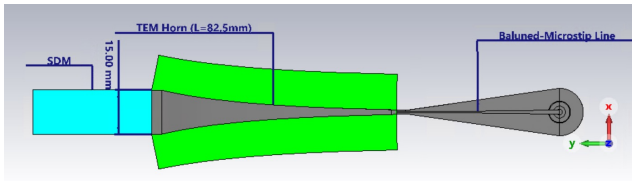

(b)

Figure 8. (a) SDM fed with TEM-horn side profile. The horn is wrapped with PMC walls at the sides; (b) feeding via microstrip line.

4 Conclusions

With self-dual radiating elements posed to solve issues that limit the scanning capabilities of phased arrays, the necessary building blocks for the accompanying feeding network have been introduced. The feasibility of new DAF and perturbed splitters and their feeding mechanism in SDM environment has been demonstrated. The results exhibit inherently good matching as expected. Our focus now is on further optimization of the existing components as well as investigating new potential components such as couplers. Additionally, other mechanisms of feeding, and potential usage of SDM as leaky-wave antenna elements and for reflect-arrays are seen possible. The realization of near-PMC media is also being investigated.

5 Acknowledgements

The authors thank Dr. Zeev Iluz for valuable assistance with CST® simulations.

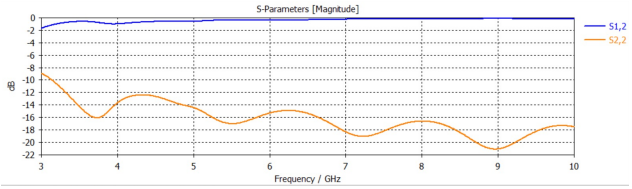

(a) S-parameters of the TEM horn itself as input impedance is transformed from 130 Ω to 377 Ω at the SDM interface.

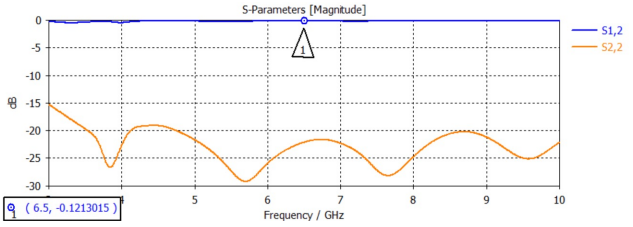

(b) S-parameters of the TEM-horn-to-SDM transition

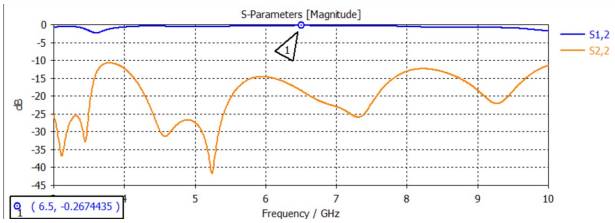

(c) Example of feeding via microstip line. S-paramteres for microstrip > TEM-horn > SDM

Figure 9. *S*-parameter performance of the microstrip to SDM transition of Fig. 8.

References

[1] N. Mohammadi Estakhri, N. Engheta, and R. Kastner, "Electromagnetic Funnel: Reflectionless Transmission and Guiding of Wave through Subwavelength Apertures," *Phys. Rev. Lett.* 124, 033901,- 22 January 2020.

[2] N. Mohammadi Estakhri, N. Engheta and R. Kastner, "Wide Scan, Wideband Arrays with Self-Dual Point-Like Elements" in *International IEEE Symposium on Antennas Propagat.*, Boston, MA, July. 8–13, 2018.

[3] R. Geva and R. Kastner, 'Obtaining a Near-Perfect Embedded Element Patterns in Phased Arrays Using Self-Dual Media", *International IEEE Symposium on Antennas Propagat.*, Denver, CO, July 10–15, 2022, To Be Presented.

[4] K. Chung, S. Pyun, and J.Choi "Design of an Ultrawide-Band TEM Horn Antenna With a Microstrip-Type Balun, "*IEEE Trans. Antennas Propagat.*, vol. 53, no. 10, pp. 3410–3413, Oct 2005.